Communication

A Triple-Band Reflective Polarization Conversion Metasurface with High Polarization Conversion Ratio for Ism and X-Band Applications

Badisa Anil Babu [1,2]ⓘ, **Boddapati Taraka Phani Madhav** [2]ⓘ, **Sudipta Das** [3]ⓘ, **Niamat Hussain** [4]ⓘ, **Syed Samser Ali** [5]ⓘ **and Nam Kim** [6,*]ⓘ

1   Department of Electronics and Communication Engineering, GMR Institute of Technology, Razam 532127, India
2   Antennas & Liquid Crystals Research Centre, Koneru Lakshmaiah Education Foundation, Vaddeswaram 522302, India
3   Department of Electronics & Communication Engineering, IMPS College of Engineering and Technology, Malda 732103, India
4   Department of Smart Device Engineering, Sejong University, Seoul 05006, Korea
5   Department of Electronics & Communication Engineering, University Institute of Technology, Burdwan 713104, India
6   Department of Information and Communication Engineering, Chungbuk National University, Cheongju 28644, Korea
*   Correspondence: namkim@chungbuk.ac.kr

Abstract: A compact and triple-band polarization converting reflective type metasurface (PCRM) with a high polarization conversion ratio (PCR) is proposed for strategic wireless antenna-integrated applications. The unit cell of the metasurface is composed of S- and G-shaped patches separated with a parasitic gap and the grounded via is connected to the full ground plane. The unit cell is etched on an FR4 substrate (dielectric constant, ε_r = 4.4, loss tangent, tan δ = 0.02), with compact dimensions of 10 mm^3 × 10 mm^3 × 1.6 mm^3. This structure provides a resonance at 5.2 (ISM), 6.9, and 8.05 GHz (X-band) frequencies. The designed unit cell structure is studied for Transverse Electric (TE)/Transverse Magnetic (TM) incident waves and their responses to the various incident angles. The corresponding PCR is calculated, which shows 92% in the lower frequency band (5.2 GHz), 93% in the second frequency band (6.9 GHz), and 94% in the high-frequency band (8.05 GHz). The total efficiency of the structure shows 83.2%, 62.95%, and 64.6% at the respective resonance bands. A prototype of the proposed PCRM with 3 × 3 unit cells is fabricated to validate the simulated results. The experimental data agrees with the simulation results. The compactness, triple-band operation with a high PCR value of more than 92% makes use of the designed metasurface in wireless antenna-integrated applications at ISM and X-bands.

Keywords: industrial scientific and medical (ISM); X-band; polarization conversion ratio (PCR); reflective metasurface (RM); triple-band

1. Introduction

Metasurfaces (MS) are artificially engineered two-dimensional structures, which have the capability of manipulating Electromagnetic (EM) propagation behavior. The MS consists of sub-wavelength periodic structures called unit cells [1,2]. The controllable characteristic parameters of EM waves are amplitude and phase. Thus, MS can be utilized for the realization of functionalities like polarization, gain control, and amplitude control [3]. The applications of these functionalities are used to realize perfect absorbers [4], frequency selective surfaces (FSS) [5], AMC reflectors and polarization converters [6] based on epsilon negative, and epsilon near to zero properties [7]. The metasurface is highly efficient in

acquiring low-profile, high-efficiency, and broadband polarization converters [8]. Polarization converters have distinct properties in controlling polarization and they have been utilized in the microwave [9], terahertz [10], and even optical [11] range of frequencies.

Polarization conversion is one of the functionalities required for current wireless devices to control polarization, gain, radar cross-section (RCS), etc. The realization of polarization converting MS can be done in two operating modes: transmission [12] and reflection [13]. Based on the type of polarization conversion, each mode is categorized into linear to circular, circular to linear, linear to linear, and cross-polarization conversion MS [14–16]. Most of the realized polarization-converting MSs are limited to broadband [17], ultra-wideband [18], wideband [19], and dual-band operation only [20]. However, to meet the current demand for wireless devices, there is a need to extend functionality to multiband. Various multifunctional and multi-polarization conversion metasurfaces were realized in the literature using different reconfiguration mechanisms [21–23]. These metasurfaces provided a challenge in terms of active component integration and the loss generated by these active components. Hence the synthesis of compact, passive polarization-converting metasurfaces have become the solution to the above challenge. Only a few works have reported on multi-band passive polarization converting MS with compact size, high polarization conversion ratio (PCR) values, and high performance [24–30].

In this paper, the design of a triple-band cross-polarization converting metasurface based on reflection is illustrated with compact dimensions and high PCR values. The unit cell structure resonates at 5.2 GHz, 6.9 GHz, and 8.05 GHz frequencies. The corresponding polarization conversion ratio is 92%, 93%, and 94%, respectively. The total efficiencies are 83.2%, 62.95%, and 64.6% at respective operating bands. For the incidence and polarization angles of the incident wave, the structure provides angular stability up to 30° incident angles, and it acts as a polarization-sensitive metasurface for polarization angles. Similarly, the characteristics of TM and TE incidents on the surface are studied. The simulated characteristics are experimentally validated using a 3×3 PCRM fabricated prototype. The compactness, high PCR, and triple-band feature make it suitable for the implementation in strategic antenna-integrated applications for ISM and X-bands.

2. Design and Simulation Analysis

2.1. Unit Cell Configuration

A schematic diagram of the reflective type cross-polarization converting metasurface with the simulated setup is shown in Figure 1a. A single-layer FR4 lossy is used as a substrate with dielectric constant (ε_r) = 4.4 and loss tangent (tan δ) = 0.002. S-and G-shaped metal patches separated with a parasitic gap and grounded via to the S-shape that makes the structure resonate at 5.2, 6.9, and 8.05 GHz. The unit cell dimensions are 10 mm^3 × 10 mm^3 × 1.6 mm^3. The geometric dimensions of the unit cell are shown in Figure 1b. The numerical simulation software CST MWS is used for design and simulated analysis.
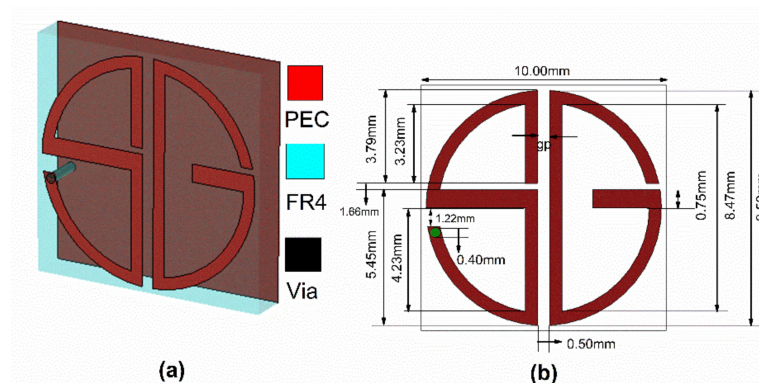

Figure 1. (**a**) Perspective view of the Unit cell; (**b**) Unit cell dimensions.

The simulation setup consists of a linearly polarized plane wave incidence in the Z-direction, while the unit cell structure lies in an XY plane. The reflected electric fields consist of co-polarization (S_{11} & S_{22}) and cross-polarization components (S_{12} & S_{21}), which are related using Equation (1):

$$\begin{bmatrix} E_x^r \\ E_y^r \end{bmatrix} = \begin{pmatrix} r_{xx} & r_{yy} \\ r_{yx} & r_{yy} \end{pmatrix} \begin{bmatrix} E_x^i \\ E_y^i \end{bmatrix} \tag{1}$$

i—incident wave; r—reflected wave; where $r_{xx} = \left| \frac{E_x^r}{E_x^i} \right|$ and $r_{yx} = \left| \frac{E_y^r}{E_x^i} \right|$.

The investigation of the cross-polarization conversion behavior of the proposed structure is carried out under linear polarized incidence. Figure 2a,b depicts the simulated reflection characteristics of the design. The structure provides three co-polarized (S_{11}) resonating bands at 5.2, 6.9, and 8.05 GHz.
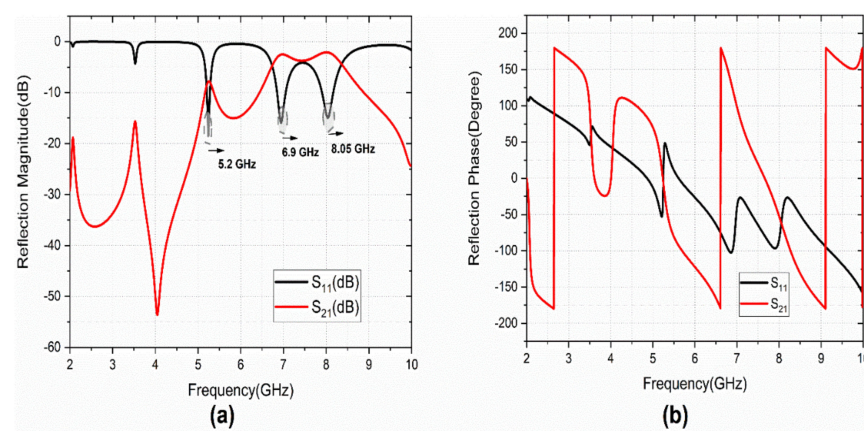

Figure 2. Simulated unit cell Co-and Cross-polarized Reflection characteristics (**a**) magnitude, (**b**) phase.

The cross-polarized reflection coefficient (S_{21}) also has peaks at operating bands. The reflection phase of the co-and cross-polarized component gives the reflected phase details for the linearly polarized incident wave. The phase difference between the co-and cross-polarized components indicates that the cross-polarization conversion mechanism of the designed metasurface to operate in triple-bands. The simulated analysis is carried out with CST MWS software. The equivalent inductance (L) and capacitance (C) values for the S-shape patch are L_s and C_s. Similarly, L_G and C_G are the equivalent values for G-shape. The L_{via} is the inductance of grounded via. Then, the resonance of the structure element is calculated as: $f_r = \frac{1}{2\pi\sqrt{LC}}$. The equivalent LC-circuit model for the design is presented in Figure 3a. The role of via in the design is studied with the simulated S_{11} (dB), as shown in Figure 3b. It is observed that the resonant frequency is lowered with triple-band operation.
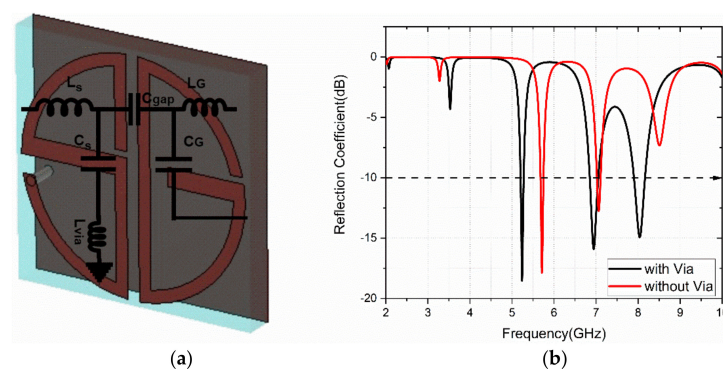

Figure 3. (**a**) Unit cell equivalent LC-circuit model representation; (**b**) Comparison of S_{11} with and without via.

The physical significance of the structure is studied using a parametric analysis of the gap (gp variable) between the S-and G-shaped patches. The simulated S_{11} and S_{21} results for gap variation are presented in Figure 4. It is observed that the optimized gap is obtained at gp = 0.5 mm for triple-band operation.
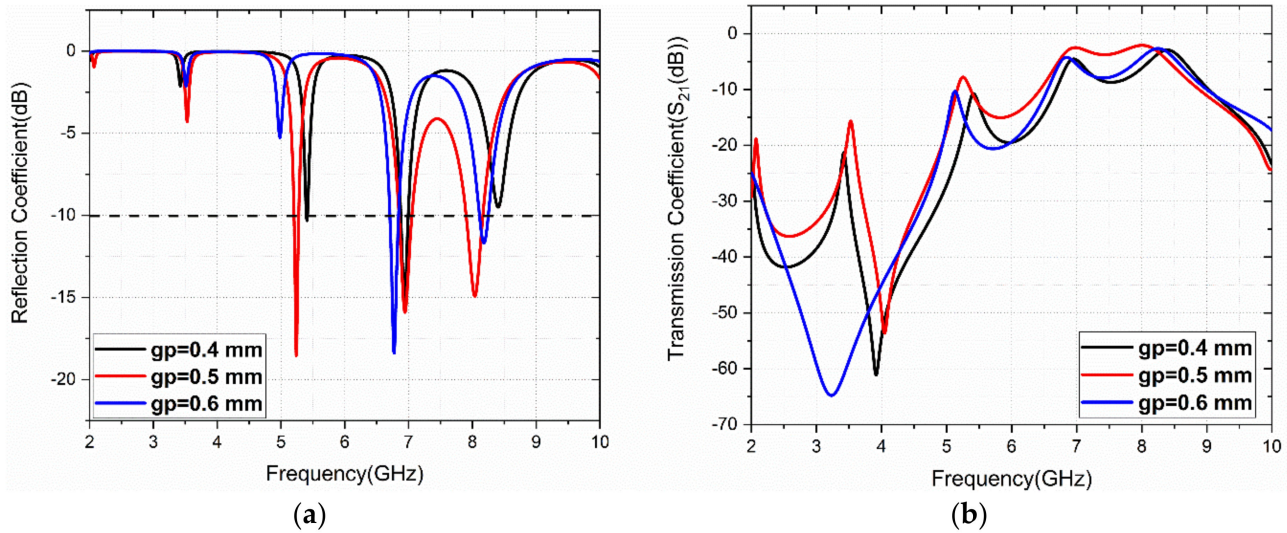

Figure 4. Parametric analysis of gap (gp) between S-and G-patches: (**a**) S_{11} (dB), (**b**) S_{21} (dB).

2.2. Response to the Incident Angle and Polarization Angle Variation

The reflection characteristics of the metasurface under different incident angles (theta) and polarization angles are studied. The simulated theta and phi variations are performed with a variation from 0° to 90° a step width of 15°. Figure 5 illustrates the co-polarized reflection characteristics. It provides angular stability of up to 30° theta variations. Figure 6 represents the reflection characteristics of the cross-polarization reflection coefficient. A few minor variations are observed with theta variation.
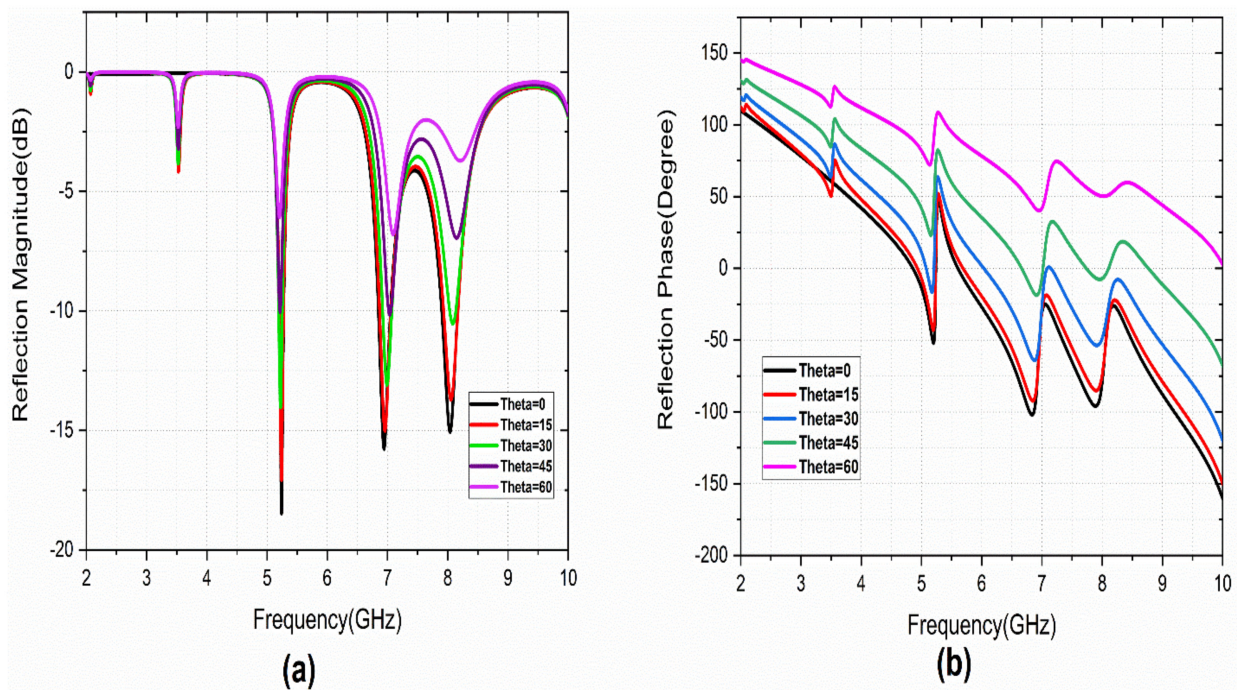

Figure 5. S_{11} variation with Theta variation: (**a**) magnitude, (**b**) phase.
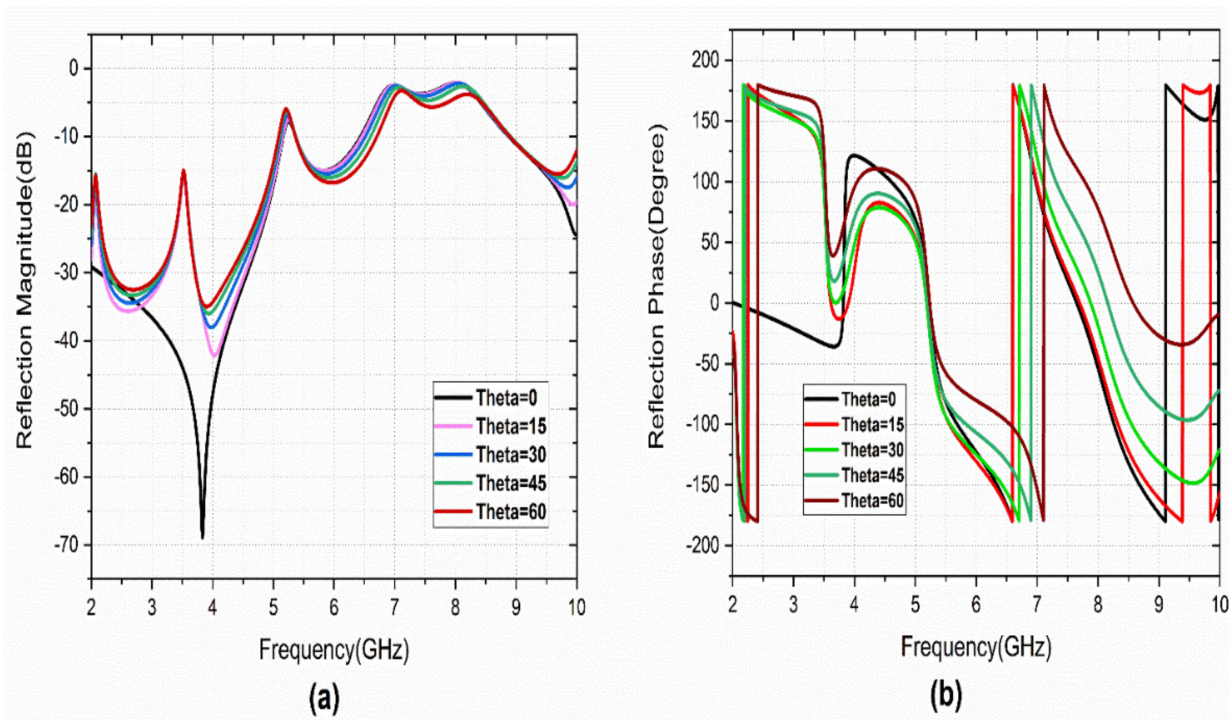
Figure 6. S_{21} variation with Theta variation: (**a**) magnitude, (**b**) phase.

The metasurface is studied further for polarization angle variation. The structure is polarization-sensitive, as the reflection characteristics are not matched with the normal incident wave. The evidence for the simulation results is shown in Figure 7. The simulation results show that the metasurface is polarization-sensitive and provides the cross-polarization conversion operation with the angular stability of 30° of incident angle.
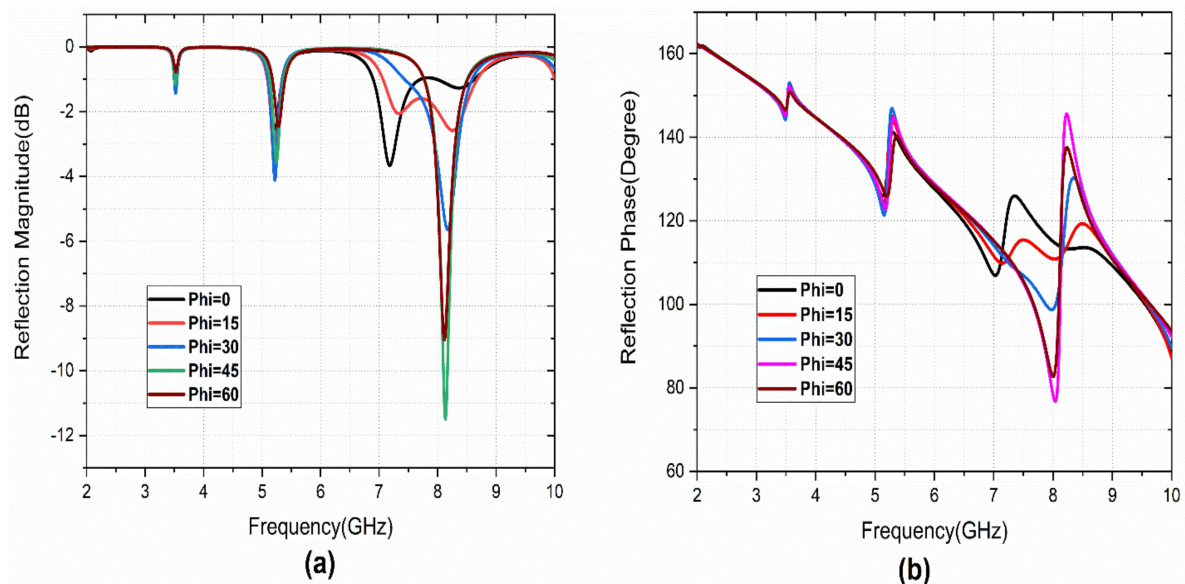

Figure 7. Reflection characteristics under Phi variation: (**a**) magnitude, (**b**) phase.

2.3. Analysis with TE and TM Incident Wave

The reflection characteristics of the PCRM with vertically polarized (TE) and horizontally polarized (TM) wave incident angle (theta) variation is studied. Figure 8 illustrates the reflection characteristics of the metasurface under TE incidence. It is observed that small variations in reflection magnitude and phase are observed. For these variations, a

corresponding variation in S_{21} is also observed, which also gives the PCRM the ability to work as a polarization converter under TE incident angle variation.
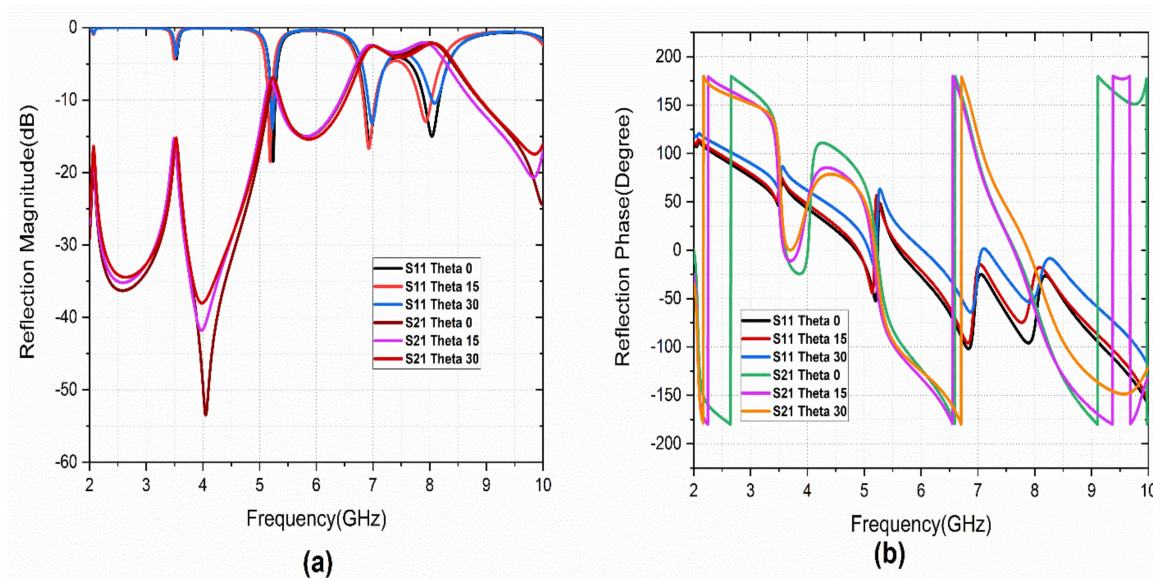

Figure 8. Reflection characteristics under TE incident angle variation: (**a**) magnitude, (**b**) phase.

Under the TM incident wave, the metasurface is affected by the fundamental mode of resonance because this resonance is provided by the magnetic resonance of the structure. For the other higher resonant frequencies, similar results are observed as in TE incident angle variations. Figure 9 shows the reflection characteristics under TM theta variation.
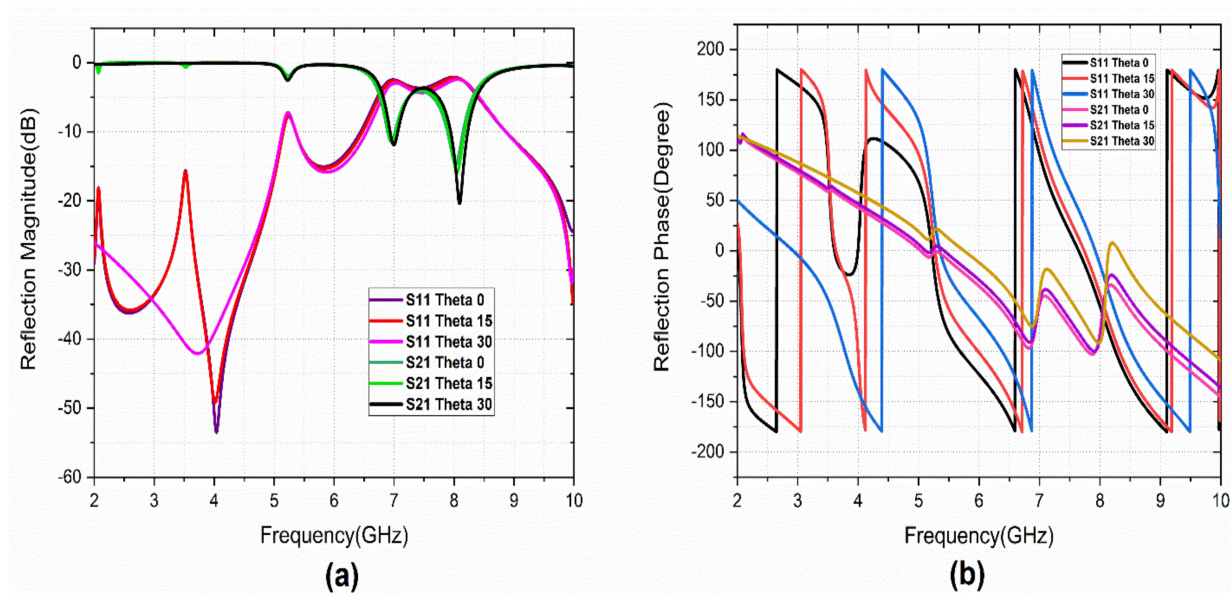

Figure 9. Reflection characteristics under TM incident angle variation: (**a**) magnitude (**b**) phase.

2.4. Analysis of Surface Current Distribution

The resonance phenomenon and the cross-polarization conversion mechanism can be studied using surface current distribution. Figure 10 illustrates the surface current distribution at the three resonant frequencies. The surface current is mostly distributed on the S-shape with the via and patch current direction being out of phase with the ground, which causes magnetic resonance at 5.2 GHz. The current intensity is on the G-shape with an in-phase current direction at 6.9 GHz, which makes electric resonance. Whereas the higher-order resonance is generated by both the S-and G-shape patches. Thus, the

lower polarization conversion band is provided by the S-shape, and the second mode is due to the G-shape and the higher mode is generated by both the S-and G-shape with the parasitic gap.
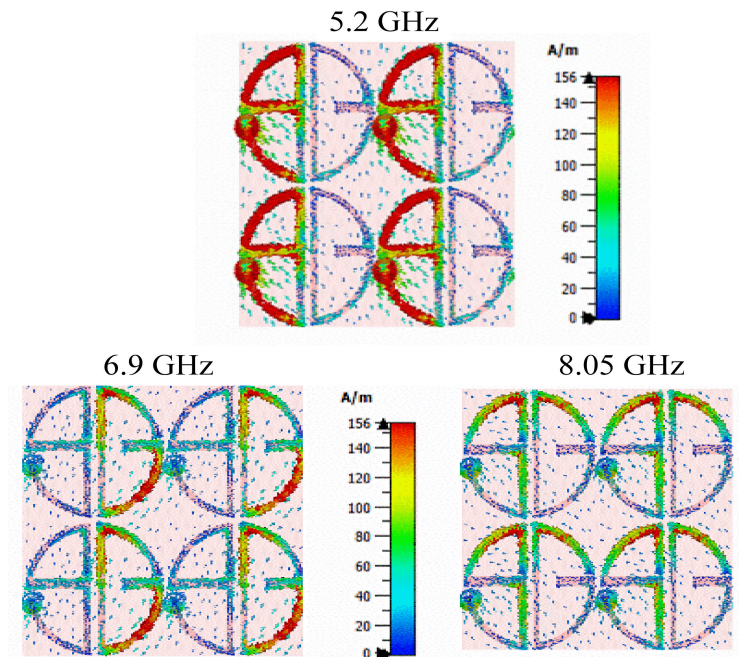
5.2 GHz

6.9 GHz   8.05 GHz

Figure 10. Simulated Surface current distribution at 5.2, 6.9, and 8.05 GHz.

Performance Analysis

The cross-polarization conversion efficiency of the design is quantified in terms of PCR. PCR can be calculated from the co-and cross-polarized reflection magnitudes as represented in Equation (2):

$$\text{PCR} = \frac{r_{yx}^2}{r_{yx}^2 + r_{xx}^2} = \frac{r_{xy}^2}{r_{xy}^2 + r_{yy}^2} \tag{2}$$

r_{yx} represents a cross-polarized component, i.e., S_{21}, and r_{xx} represents the co-polarization component, i.e., S11. The highest polarization conversions obtained are 92% for the first operating band, 94% for the second operating band, and 93% for the third operating band under normal incidence. The PCR variation with oblique angles of the incident wave (theta) is also calculated and presented in Figure 11. Incident angles of up to 30° provides a PCR value of more than 85%.
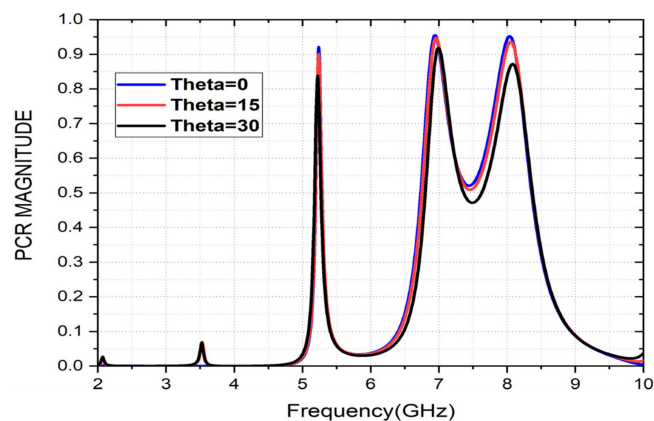

Figure 11. PCR Variation for various incident angles (theta).

3. Experimental Setup and Results

To validate the design, a 3 × 3 experimental sample was fabricated and measured, and the co-and cross-polarization reflection characteristics were calculated, as well as the PCR value. The fabricated sample is given in Figure 12. The schematic diagram of the experimental setup for characterization is shown in Figure 13. Anritsu MS2037C VNA and two standard horn antennas were used as transmitters and receivers with x-and y-polarization. The measured and calculated results agreed well. The observed variations in measured results were due to fabrication and measurement errors only. Figure 14 shows the comparison between simulated and measured results of the reflection magnitude and PCR under the normal incidence of the incoming wave. The variation in measured results was due to fabrication errors and size limitations of the prototype in the measurement setup. The measured results were taken at normal incidence angles.
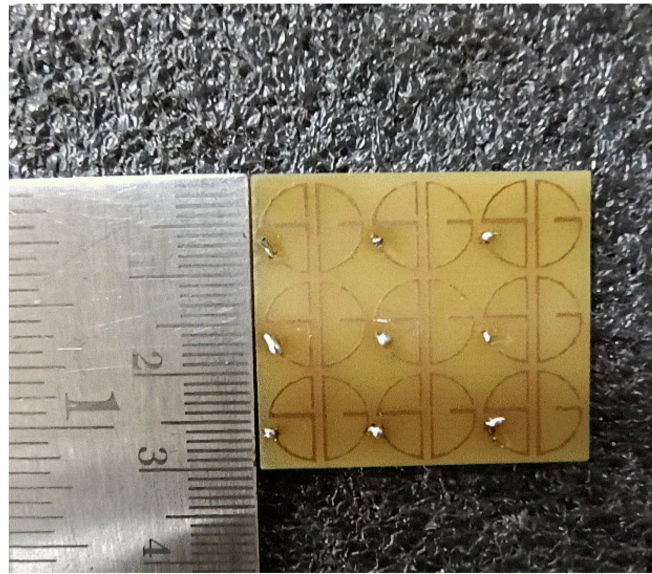

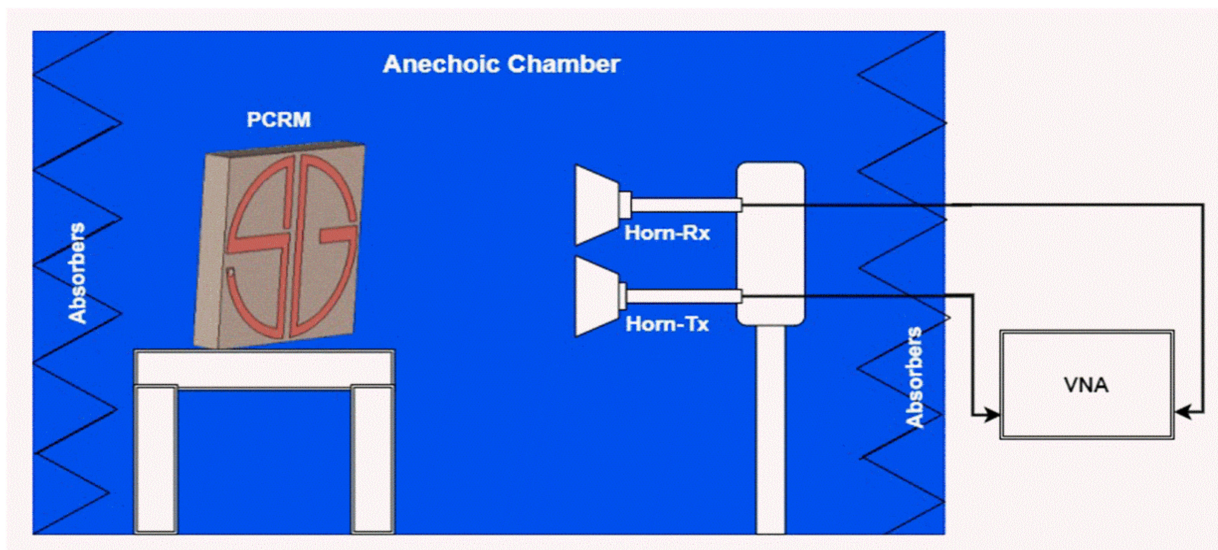**Figure 12.** Fabricated 3 × 3-unit cell prototype.

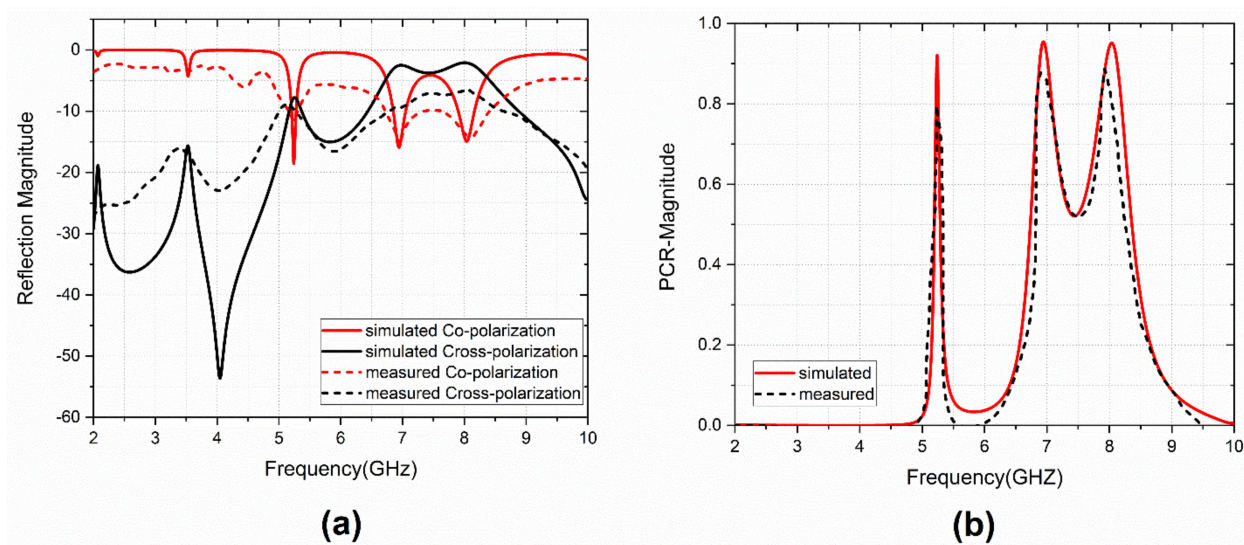**Figure 13.** Schematic of the measurement setup.

Figure 14. Comparison between simulated and measured results: (**a**) reflection magnitude, (**b**) PCR.

The simulated and measured total efficiency is shown in Figure 15. The measured data shows similar efficiency curves as the numerically computed total efficiency. However, the measured efficiency was observed to be a little lower than the simulated values due to substrate losses.
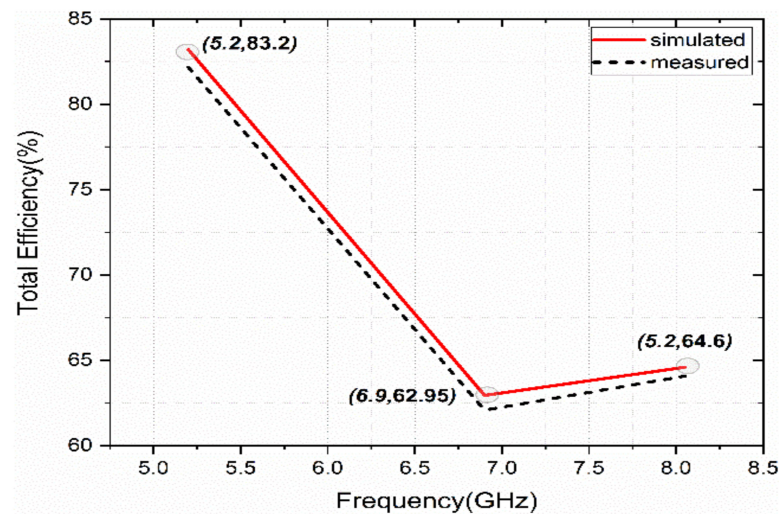

Figure 15. Total efficiency as a function of frequency.

Table 1 presents a comparison of the designed triple-band reflective cross-polarization converter with the state-of-the-art related works reported in the literature. It can be observed that the proposed metasurface provides a triple-band operation with a relatively compact size. The structure consists of parasitic patch elements with grounded via that acted as a cross-polarization converter with PCR of >92%. Moreover, it offers high PCR values, which is one of the essential requirements for the current wireless communication systems. The physical mechanism of the realized structure is verified using numerical simulations and experimental characterization of a 3 × 3 array sample. There are few works that have a smaller size [24,29]. However, ref. [24] did not perform an analysis of PCR, while ref. [29] has lower PCR values.

Table 1. Comparison with other related works.

Ref. No	Substrate	Unit Cell Size (L × W × h) λ_0^3	PCR (%)	Frequency (GHz)	Conversion Type
[24]	FR4	0.128 × 0.128 × 0.128	–	9.1–16.5, 20–25.4, 17.4–18.9	Cross-polarization LP-CP
[25]	FR4	0.19 × 0.19 × 0.049	>86	4.47–5.35 9.45–13.60	Cross-polarization LP-CP LP-LP
[26]	F4B	0.285 × 0.285 × 0.071	>90	10.75, 19.65, 27.35	Cross-polarization LP-LP
[27]	RT Duroid 4730	0.186 × 0.186 × 0.055	≥80	4.34–4.98, 6.77–6.97, 8.25–8.69, 10.72–15.56	Cross-polarization LP-CP
[28]	F4B-2	0.28 × 0.28 × 0.084	≥90	4.60–12.27, 13.79–13.90, 14.61–14.69, 15.44–15.52	Cross-polarization LP-LP
[29]	F4B	0.152 × 0.152 × 0.038	>90	5.7,8.8,14.85	Multi polarization CP-LP, LP-CP LP-LP
[30]	Rogers RO 40003	0.5 × 60.56 × 0.034	>90	5.30–5.41, 5.77–7.58, 9.27–13.91, 17.53–19.59	Multifunctional LP-LP LP-CP
Prop. Work	FR4	0.173 × 0.173 × 0.027	>92	5.2, 6.9, 8.05	Cross-Polarization LP-LP

λ_0 is the center fundamental frequency wavelength, LP—Linear Polarization, CP—Circular Polarization.

4. Conclusions

In this article, a triple-band, compact PCRM is designed, and its characteristics are studied under incidence and polarization angles. The physical significance of the structural elements is presented along with an equivalent LC-circuit model representation and a detailed parametric analysis. The simulated results show that it provides angular stability of up to 300 of incidence angle and is sensitive to the polarization angle. It provides PCR values of 92%, 93%, and 94% at 5.2, 6.9, and 8.05 GHz. The PCR values under TE and TM modes are also calculated, and the operating mechanism is demonstrated through surface current distribution. The total efficiency of reflecting PCRM is 83.2%, 62.95%, and 64.6%, at resonating bands. These results are compared with the existing triple-band reflecting metasurface in terms of angular stability, unit cell size, and PCR. The features, such as compactness and triple-band operation with PCR values, have strategic antenna-integrated applications for ISM and X-band communications.

Author Contributions: Conceptualization: B.A.B. and B.T.P.M.; methodology: B.A.B. and S.D.; software: B.A.B. and N.H.; validation: S.D.; B.T.P.M. and S.S.A.; formal analysis: N.H. and S.S.A.; writing—original draft preparation: B.A.B.; B.T.P.M. and S.D.; writing—review, and editing: N.H.; S.S.A. And N.K.; supervision: B.T.P.M. and N.K.; Project administration: N.K. All authors have read and agreed to the published version of the manuscript.

Institutional Review Board Statement: Not applicable.

Informed Consent Statement: Not applicable.

Data Availability Statement: Not applicable.

Conflicts of Interest: The authors declare no conflict of interest.

References

1. Bukhari, S.S.; Vardaxoglou, J.; Whittow, W. A Metasurfaces Review: Definitions and Applications. *Appl. Sci.* **2019**, *9*, 2727. [CrossRef]
2. Hsu, W.-L.; Chen, Y.-C.; Yeh, S.P.; Zeng, Q.-C.; Huang, Y.-W.; Wang, C.-M. Review of Metasurfaces and Meta devices: Advantages of Different Materials and Fabrications. *Nanomaterials* **2022**, *12*, 1973. [CrossRef]
3. Zhang, L.; Mei, S.; Huang, K.; Qiu, C.-W. Advances in Full Control of Electromagnetic Waves with Metasurfaces. *Adv. Opt. Mater.* **2016**, *4*, 818–833. [CrossRef]
4. Liang, Y.; Lin, H.; Koshelev, K.; Zhang, F.; Yang, Y.; Wu, J.; Kivshar, Y.; Jia, B. Full-stokes polarization perfect absorption with diatomic metasurfaces. *Nano Lett.* **2021**, *21*, 1090–1095. [CrossRef]
5. Alwareth, H.; Ibrahim, I.M.; Zakaria, Z.; Al-Gburi, A.J.A.; Ahmed, S.; Nasser, Z.A. A wideband high-gain microstrip array antenna integrated with frequency-selective surface for Sub-6 GHz 5G applications. *Micromachines* **2022**, *13*, 1215. [CrossRef]
6. Sun, Z.; Liu, R.; Cao, H.; Gong, H.; Du, M.; Li, S. Dual-Axis Metasurface Strain Sensor Based on Polarization–Phase-Deformation Relationship. *Sensors* **2020**, *20*, 1307. [CrossRef]
7. Pang, K.; Alam, M.Z.; Zhou, Y.; Liu, C.; Reshef, O.; Manukyan, K.; Voegtle, M.; Pennathur, A.; Tseng, C.; Su, X.; et al. Adiabatic frequency conversion using a time-varying epsilon-near-zero metasurface. *Nano Lett.* **2021**, *21*, 5907–5913. [CrossRef]
8. Majeed, A.; Zhang, J.; Ashraf, M.A.; Memon, S.; Mohammadani, K.H.; Ishfaq, M.; Sun, M. An Ultra-Wideband Linear-to-Circular Polarization Converter Based on a Circular, Pie-Shaped Reflective Metasurface. *Electronics* **2022**, *11*, 1681. [CrossRef]
9. Sakda, N.; Chitaree, R.; Rahman, B.M.A. Reflective Terahertz Metasurfaces Based on Non-Volatile Phase Change Material for Switchable Manipulation. *Photonics* **2022**, *9*, 508. [CrossRef]
10. Rahman, B.M.A.; Viphavakit, C.; Chitaree, R.; Ghosh, S.; Pathak, A.K.; Verma, S.; Sakda, N. Optical Fiber, Nanomaterial, and THz-Metasurface-Mediated Nano-Biosensors: A Review. *Biosensors* **2022**, *12*, 42. [CrossRef] [PubMed]
11. Ullah, N.; Zhao, R.; Huang, L. Recent Advancement in Optical Metasurface: Fundament to Application. *Micromachines* **2022**, *13*, 1025. [CrossRef] [PubMed]
12. Li, X.; Wang, Y.; Fan, J.; He, J.; Huang, X. Ultra-Thin/Wide-Band Polarization Conversion Metasurface and Its Applications in Anomalous Reflection and RCS Reduction. *Appl. Sci.* **2022**, *12*, 7696. [CrossRef]
13. Sui, R.; Wang, J.; Xu, Y.; Feng, D. An X-Band Reflective Active Polarization Conversion Metasurface. *Electronics* **2022**, *11*, 2847. [CrossRef]
14. Mohanty, A.; Behera, B.R.; Esselle, K.P.; Alsharif, M.H.; Jahid, A.; Mohsan, S.A.H. Investigation of a Dual-Layer Metasurface-Inspired Fractal Antenna with Dual-Polarized/-Modes for 4G/5G Applications. *Electronics* **2022**, *11*, 2371. [CrossRef]
15. Tian, Y.; Han, L.; Yan, L.; Wang, J.; Zhang, B.; Jiao, Z. Optically Controlled Terahertz Multifunctional Polarization Conversion Metasurface with Reflection and Transmission Modes. *Micromachines* **2022**, *13*, 1387. [CrossRef] [PubMed]
16. Ahmad, T.; Rahim, A.A.; Bilal, R.M.H.; Noor, A.; Maab, H.; Naveed, M.A.; Madni, A.; Ali, M.M.; Saeed, M.A. Ultrawideband Cross-Polarization Converter Using Anisotropic Reflective Metasurface. *Electronics* **2022**, *11*, 487. [CrossRef]
17. Mao, C.; Yang, Y.; He, X.; Zheng, J.; Zhou, C. Broadband Reflective Multi-Polarization Converter Based on Single-Layer Double-L-Shaped Metasurface. *Appl. Phys. A* **2017**, *123*, 767. [CrossRef]
18. Gao, X.; Han, X.; Cao, W.-P.; Li, H.O.; Ma, H.F.; Cui, T.J. Ultrawideband and High-Efficiency Linear Polarization Converter Based on Double V-Shaped Metasurface. *IEEE Trans. Antennas Propag.* **2015**, *63*, 3522–3530. [CrossRef]
19. Zheng, Q.; Guo, C.; Ding, J. Wideband Metasurface-Based Reflective Polarization Converter for Linear-to-Linear and Linear-to-Circular Polarization Conversion. *IEEE Antennas Wirel. Propag. Lett.* **2018**, *17*, 1459–1463. [CrossRef]
20. Kamal, B.; Chen, J.; Yin, Y.; Ren, J.; Ullah, S.; Ali, U. Design and Experimental Analysis of Dual-Band Polarization Converting Metasurface. *IEEE Antennas Wirel. Propag. Lett.* **2021**, *20*, 1409–1413. [CrossRef]
21. Wu, P.C.; Zhu, W.; Shen, Z.X.; Chong, P.H.J.; Ser, W.; Tsai, D.P.; Liu, A.-Q. Broadband wide-angle multifunctional polarization converter via liquid-metal-based metasurface. *Adv. Opt. Mater.* **2017**, *5*, 1600938. [CrossRef]
22. Li, W.; Xia, S.; He, B.; Chen, J.; Shi, H.; Zhang, A.; Li, Z.; Xu, Z. A Reconfigurable Polarization Converter Using Active Metasurface and Its Application in Horn Antenna. *IEEE Trans. Antennas Propag.* **2016**, *64*, 5281–5290. [CrossRef]
23. Sun, S.; Jiang, W.; Gong, S.; Hong, T. Reconfigurable Linear-to-Linear Polarization Conversion Metasurface Based on PIN Diodes. *IEEE Antennas Wirel. Propag. Lett.* **2018**, *17*, 1722–1726. [CrossRef]
24. Liu, X.; Zhang, J.; Li, W.; Lu, R.; Li, L.; Xu, Z.; Zhang, A. Three-Band Polarization Converter Based on Reflective Metasurface. *IEEE Antennas Wirel. Propag. Lett.* **2017**, *16*, 924–927. [CrossRef]
25. Huang, X.; Yang, H.; Zhang, D.; Luo, Y. Ultrathin Dual-Band Metasurface Polarization Converter. *IEEE Trans. Antennas Propag.* **2019**, *67*, 4636–4641. [CrossRef]
26. Yang, Z.; Yu, S.; Kou, N.; Long, F.; Ding, Z.; Zhang, Z. Ultrathin Tri-Band Reflective Cross-Polarization Artificial Electromagnetic Metasurface. *J. Electromagn. Waves Appl.* **2020**, *34*, 1491–1501. [CrossRef]

27. Lin, B.Q.; Guo, J.X.; Chu, P.; Huo, W.J.; Xing, Z.; Huang, B.G.; Wu, L. Multiple-band Linear-Polarization Conversion and Circular Polarization In Reflection Mode Using Asymmetric Anisotropic Metasurface. *Phys. Rev. Appl.* **2018**, *9*, 024038. [CrossRef]

28. Wu, L.P.; Fang, Q.H.; Pan, W.K.; Li, M.H.; Dong, J.F. Realization of Cross-Polarization Conversion for Linearly Polarized Waves in Multiband by Orthotropic Metasurface. *J. Electromagn. Waves Appl.* **2022**, *36*, 101–114. [CrossRef]

29. Yuan, L.; Hou, L.; Zhang, Z. Triple-Band Highly Efficient Multi-Polarization Converter Based on Reflective Metasurface. *Prog. Electromagn. Res. M* **2021**, *102*, 127–135. [CrossRef]

30. Ghosh, S.; Ghosh, J.; Singh, M.S.; Sarkhel, A. A Low-Profile Multifunctional Metasurface Reflector for Multiband Polarization Transformation. *IEEE Trans. Circuits Syst. II Express Briefs* **2022**. [CrossRef]